Periodic band structure calculation by the Sakurai-Sugiura method with a fast direct solver for the boundary element method with the fast multipole representation

Hiroshi Isakari[a], Toru Takahashi[a], Toshiro Matsumoto[a]

[a]*Nagoya University, Japan*

Abstract

In this paper, we present a numerical method for periodic band structure calculation, which is associated with eigenvalue problems for periodic problems, using the boundary element method (BEM). In the BEM, the eigenvalue problems are converted into non-linear eigenvalue problems, which are not tractable with conventional eigensolvers. In the present study, to solve non-linear eigenvalue problems, the block Sakurai–Sugiura (SS) method, which can convert non-linear eigenvalue problems into generalised eigenvalue problems, is utilised. A fast direct solver for the BEM with a fast multipole representation is employed in the algorithm of the block SS method since algebraic equations need to be solved for multiple right–hand sides in the block SS method. We conduct several numerical experiments related to phononic structures to confirm the validity and efficiency of the proposed method. We confirm that the proposed method can calculate the band structure of the phononic structures, and the computational time with the proposed method is less than that with a conventional FEM-based eigensolvers with triangular linear elements even for relatively small problems.

Keywords: Photonic/Phononic band structure, Periodic problem, Sakurai–Sugiura method, Non-linear eigenvalue problem, Fast direct solver for boundary element method, Fast multipole method

1. Introduction

In the last several decades, periodic structures such as photonic and phononic crystals have attracted considerable attention of researchers and engineers [1]. This is because these materials have complete bandgaps for waves. A complete bandgap is defined as a frequency range in which waves cannot propagate in any direction. A periodic dielectric material which has bandgaps for an electromagnetic wave (including light) is called a photonic crystal and its elastic counterpart is called a phononic crystal or structure. These materials are expected to be used in the next generation of wave devices, such as lasers, waveguides, and slow light in the field of optics and acoustic filters, noise controling devices, and transducers in the field of mechanics. To realise these technologies, it is important to develop a fast and accurate numerical solver for bandgap calculations.

Several numerical methods for bandgap calculations have been proposed. As classical methods, we can mention plane wave expansion (PWE) [2, 3] and the multiple scattering theory (MST) [4, 5]. The applicability of these methods is limited to problems with simple geometry. As general methods for bandgap calculations, although the finite difference in time domain (FDTD) method and the finite element method (FEM) are widely used, the applicability of these methods may not be sufficient for realistic engineering problems in some cases. The FDTD requires the discretisation of the whole domain, which makes it difficult to apply this method to large-scale photonic/phononic simulations, particularly in three-dimensional domain. Further, since FDTD is a method to solve the wave equation in the time domain, we need to calculate wave propagation for sufficiently long period of time for waves containing various frequencies, and convert the obtained wave distribution into the spectrum domain, which may be time consuming, particularly for three-dimensional problems with a complex geometry. Although the FEM can directly solve the eigenvalue problems in the frequency domain, it still suffers from domain discretisation. It is known that, when hp-FEM is used to calculate eigenvalues for partial differential equations (PDEs), the eigenvalues converge exponentially as the degree of freedom (DoF) increases [6]. Although the exponential convergence is attractive, hp-FEM is, to the knowledge of the authours, not necessarily widely used for band structure calculation. This is partly because the implementation of the hp-FEM is relatively complicated, and the mesh discretisation cost is expensive for complicated geometry.

As a possible alternative for numerical bandgap calculations, we can mention the boundary element method (BEM). We, however, encounter non-linear eigenvalue problems which are not tractable with conventional eigensolvers when we naively employ the BEM to reformulate the eigenvalue problems related to periodic problems. Irrespective of its difficulty to deal with the non-linear eigenvalue problem, some researchers have proposed bandgap calculations with the BEM [7, 8, 9, 10]. These methods are classified into the following two categories:

- Consider the frequency ω as a given parameter and the Bloch wave vector k as an eigenvalue.
- Consider the Bloch wave vector k as a given parameter and the frequency ω as an eigenvalue,

The former gives a generalised (resp. quadratic) eigenvalue problem for a square (resp. triangular) lattice, while the latter gives a non-linear eigenvalue problem [7]. Li et al. [7, 8] used the former approach, and successfully solved photonic/phononic band structures by relaxing the periodic boundary condition to ensure numerical stability. [9] is also considered as the former approach, in which a Dirichlet-to-Neumann map is utilised. As an example of the latter method, Barnett and Greengard [10] presented an efficient evaluation of the Green function, which satisfies the periodic boundary condition, and its application to bandgap calculations. Since they focused on the evaluation of the periodic Green function, they simply plotted the smallest singular value of the relevant matrix to find the eigenvalue. Thus, there are few studies on an effective numerical method to solve the non-linear eigenvalue problem stemming from the latter approach.

Recently, some promissing solvers for non-linear eigenvalue problems are developed; Sakurai–Sugiura (SS) method [11, 12], non-linear Arnoldi method [13] and the infinite Arnoldi method [14]. Among them, the SS method shall be used in this paper. Sakurai and Sugiura originally proposed the SS method to find certain eigenvalues of a generalised eigenvalue problem that lie in a given

domain of the complex plane [11], and Asakura et al. pointed out the possibility that the SS method can solve a non-linear eigenvalue problem [12]. Since its development, applications of the SS method are rapidly enhanced. The SS method is, thus far, applied to the calculations of the core-excited state of formaldehyde [15], eigenvalue problems in lattice quantum chromodynamics (QCD) [16], eigenvalue problems in 2D and 3D Helmholtz' equations [17, 18], eigenvalue problems related waveguides [19], etc. Also, as a similar method to the SS method, we can mention the method by Beyn [20]. In our previous paper [21], we have attempted to apply the SS method to calculate the bandgap for a phononic structure in 2D. Since the conventional BEM without any acceleration technique is combined with the SS method in [21], we have calculated bandgaps for a simple phononic structure which has a circular scatterer in the unit cell. In order to deal with a more complex geometry, in this paper, we present a combination of an accelerated BEM with the SS method.

In the algorithm of the SS method, when multiple eigenvalues are concerned, we need to solve algebraic equations with multiple right-hand sides (block SS method). Because of the multiple right-hand sides, the use of the widely used fast multipole boundary element method (FMBEM) [22, 23], which involves iterative solvers for algebraic equations, may not accelerate the eigensolver. In such a case, it is preferable to use a direct solver rather than an iterative solver to solve the algebraic equations. Thus far, some fast direct solvers, in which algebraic equations of size N obtained as a discretised boundary integral equation can be solved by a direct solver with an $O(N \log^{\alpha} N)$, $(\alpha = 0, 1, 2)$ computational complexity, have been proposed [24, 25]. In this study, we utilise a direct solver for the BEM with a fast multipole representation [26], which is henceforth denoted as "direct FMM". Although the direct FMM might not achieve $O(N \log^{\alpha} N)$ complexity for large N, it is relatively easy to implement and is efficient for moderately sized problems. Thus, our main focus in this paper is to accelerate bandgap calculations with the BEM and the SS method for 2D photonic/phononic crystals with a relatively complex geometry which can be modelled with moderate N.

The rest of the paper is organised as follows: After eigenvalue problems related to photonic/phononic crystals and its reformulation with the boundary integral equation are stated in Sections 2.1 and 2.2, respectively, the formulation the SS method is reviewed in Section 2.3. In Sections 2.4 and 2.5, we present the formulation of the direct FMM and its extension for periodic problems. In Section 3, we show some numerical examples to show the validity and the efficiency of the proposed method.

Although we focus on orthotropic periodic problems in this paper, other general periodic problems can be appropriately formulated with minor modifications.

2. Formulation

2.1. Statement of the eigenvalue problem associated with periodic structures

We consider a doubly orthotropic periodic array of scatterers in elastic matrix Ω embedded in the unit cell $U := \{x \mid 0 < x_i < L_i,\ i = 1, 2\}$, where L_i denotes the period along the x_i axis (Figure 1). Let $u(x)$ be an out-of-plane time harmonic displacement satisfying the following

Helmholtz equation:

$$\nabla^2 u(x) + \omega^2 \frac{\rho}{\mu} u(x) = 0 \quad x \in \Omega, \tag{1}$$

where ρ, μ and ω denote the density, the shear modulus and the angular frequency, respectively. We are interested in finding ω with which a non-trivial function u satisfies the Helmholtz equation (1) along with the following homogeneous boundary conditions:

$$u(x) = 0 \quad x \in \Gamma_u, \tag{2}$$

$$q(x) := \frac{\partial u(x)}{\partial n} = 0 \quad x \in \Gamma_q, \tag{3}$$

and the following quasi-periodic boundary conditions:

$$u(x + a_i) = u(x) \exp(\mathrm{i} k \cdot a_i) \quad x \in \Gamma_{\mathrm{I}}, \tag{4}$$

$$\frac{\partial u}{\partial x_i}(x + a_i) = \frac{\partial u}{\partial x_i}(x) \exp(\mathrm{i} k \cdot a_i) \quad x \in \Gamma_{\mathrm{I}}, \tag{5}$$

where $\Gamma_u \subset \Gamma_{\mathrm{B}} := \partial\Omega$ and $\Gamma_q := \Gamma_{\mathrm{B}} \setminus \overline{\Gamma_u}$ denote Dirichlet and the Neumann boundary, respectively. Γ_{I} represents a part of the boundary of U defined as $\Gamma_{\mathrm{I}} := \cup_{i=1,2}\Gamma_{\mathrm{I}i}$, $\Gamma_{\mathrm{I}i} = \{x \mid 0 < x_{3-i} < L_{3-i},\ x_i = 0,\ i = 1, 2\}$. We also define Γ_{D} and $\Gamma_{\mathrm{D}i}$ as $\Gamma_{\mathrm{D}} = \{x \mid x - a_i \in \Gamma_{\mathrm{I}},\ i = 1, 2\}$ and $\Gamma_{\mathrm{D}i} = \{x \mid x - a_i \in \Gamma_{\mathrm{I}i}\}$, respectively. $a_i = ((2 - i)L_i, (i - 1)L_i)^t \in \mathbb{R}^2$ and $\mathsf{k} = (k_1, k_2)^t \in \mathbb{R}^2$ denote the lattice vector and the Bloch wave vector, respectively. n indicates the outward unit normal of Ω defined on $\Gamma := \overline{\Gamma_{\mathrm{B}} \cup \Gamma_{\mathrm{I}} \cup \Gamma_{\mathrm{D}}}$. We henceforth denote such ω that satisfies the boundary value problem (1)–(5) with a non-trivial u as the eigenvalue. As indicated, for example, in [6], the eigenvalue problem (1)–(5) has only real eigenvalues. By solving the eigenvalue problem for all k on the edge of the reduced first Brillouin zone (Figure 2), we can obtain the band diagram of the periodic structures. In practice, we explore several eigenvalues with small magnitude. Although we have formulated the periodic eigenvalue problem with the elastodynamic notations, the formulation can be interpreted as a two-dimensional electromagnetic problem by replacing μ/ρ with the permittivity ε.

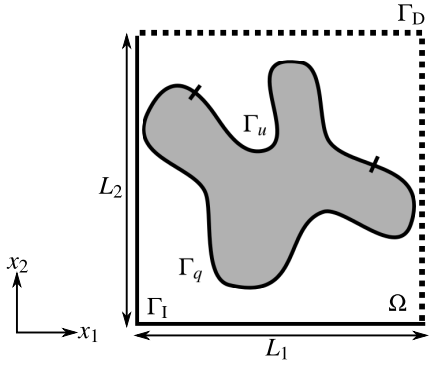

Figure 1: Periodic problem.

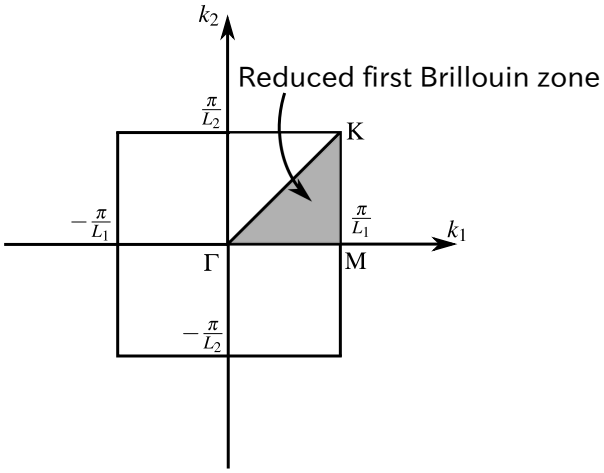

Figure 2: Reduced first Brillouin zone.

2.2. Boundary integral formulation

The eigenvalue problem (1)–(5) can be reformulated with the following boundary integral equations:

$$c(x)u(x) + (\mathcal{D}_{\Gamma_q \cup \Gamma_\mathrm{I}} u)(x) + \sum_{i=1}^{2} (\widetilde{\mathcal{D}}_{\Gamma_{\mathrm{D}i}} u)(x) = (\mathcal{S}_{\Gamma_u \cup \Gamma_\mathrm{I}} q)(x) - \sum_{i=1}^{2} (\widetilde{\mathcal{S}}_{\Gamma_{\mathrm{D}i}} q)(x) \quad x \in \Gamma, \tag{6}$$

where $\mathcal{S}_\Gamma$, $\mathcal{D}_\Gamma$, $\widetilde{\mathcal{S}}_{\Gamma_{\mathrm{D}i}}$ and $\widetilde{\mathcal{D}}_{\Gamma_{\mathrm{D}i}}$ denote integral operators defined as follows:

$$(\mathcal{S}_\Gamma q)(x) = \int_{y \in \Gamma} G(x-y) q(y) \mathrm{d}S(y), \tag{7}$$

$$(\mathcal{D}_\Gamma u)(x) = \int_{y \in \Gamma} \frac{\partial G(x-y)}{\partial n(y)} u(y) \mathrm{d}S(y), \tag{8}$$

$$(\widetilde{\mathcal{S}}_{\Gamma_{\mathrm{D}i}} q)(x) = \int_{y \in \Gamma_{\mathrm{D}i}} G(x-y) \exp(\mathrm{i}k \cdot a_i) q(y - a_i) \mathrm{d}S(y), \quad i = 1, 2, \tag{9}$$

$$(\widetilde{\mathcal{D}}_{\Gamma_{\mathrm{D}i}} u)(x) = \int_{y \in \Gamma_{\mathrm{D}i}} \frac{\partial G(x-y)}{\partial n(y)} \exp(\mathrm{i}k \cdot a_i) u(y - a_i) \mathrm{d}S(y), \quad i = 1, 2, \tag{10}$$

where $G(x-y)$ indicates the free-space Green function for the Helmholtz equation in 2D, which has the following representation:

$$G(x-y) = \frac{\mathrm{i}}{4} H_0^{(1)} \left(\omega \sqrt{\frac{\rho}{\mu}} |x-y| \right), \tag{11}$$

where $H_n^{(1)}$ denotes the Hankel function of the first kind and order n. Further, $c(x)$ in Eq. (6) represents the free term of the boundary integral equation which is equal to $1/2$ when Γ is smooth on x. Note that all unknown density functions can be written in terms of u on Γ_q, q on Γ_u, and u, q on Γ_I since $\forall y \in \Gamma_{\mathrm{D}i}, y - a_i \in \Gamma_{\mathrm{I}i}$ $(i = 1, 2)$ holds.

Our eigenvalue problem is now defined as "to find ω with which the integral equation (6) has a non-trivial solution u". Note that the eigenvalue ω is included in Eq. (11) non-linearly due to the non-linearity of the Green function.

2.3. Sakurai-Sugiura method

In this study, we utilise the Sakurai-Sugiura (SS) method [12] to solve the non-linear eigenvalue problem associated with the boundary integral equation (6) which is discretised by the collocation method into the following algebraic equations:

$$\mathsf{A}(\omega)\psi = 0, \tag{12}$$

where $\mathsf{A}(\omega) \in \mathbb{C}^{N\times N}$ denotes the influence coefficient matrix which is obtained as one discretises the integral operators (7)–(10), N indicates the number of boundary elements, and $\psi \in \mathbb{C}^N$ consists of u and q on collocation points on $\overline{\Gamma_{\mathrm{B}} \cup \Gamma_{\mathrm{I}}}$. With the SS method, we can convert the non-linear eigenvalue problem associated with (12) into a generalised eigenvalue problem, which is tractable with conventional eigensolvers such as LAPACK routines. In the rest of this section, we briefly review the formulation of the SS method. The reader is referred to the original paper [12] and/or our previous papers [17, 18] for further details.

Let us define the following function $f(z)$ for $z \in \mathbb{C}$:

$$f(z) = \mathsf{u}^H \mathsf{A}^{-1}(z)\mathsf{v}, \tag{13}$$

where u, $\mathsf{v} \in \mathbb{C}^N$ denote arbitrary non-zero vectors. With the function $f(z)$, the moments μ_j are defined as follows:

$$\mu_j = \frac{1}{2\pi \mathrm{i}} \int_{z\in\gamma} z^j f(z)\mathrm{d}z, \tag{14}$$

where γ denotes a positively orientated closed Jordan curve in the complex plane and $j \in \mathbb{N}$. Two Hankel matrices H_m and $\mathsf{H}_m^<$ composed of the moments μ_j are, respectively, defined as follows:

$$\mathsf{H}_m = \begin{pmatrix} \mu_0 & \mu_1 & \cdots & \mu_{m-1} \\ \mu_1 & \mu_2 & \cdots & \mu_m \\ \vdots & \vdots & \ddots & \vdots \\ \mu_{m-1} & \mu_m & \cdots & \mu_{2m-2} \end{pmatrix}, \tag{15}$$

$$\mathsf{H}_m^< = \begin{pmatrix} \mu_1 & \mu_2 & \cdots & \mu_m \\ \mu_2 & \mu_3 & \cdots & \mu_{m+1} \\ \vdots & \vdots & \ddots & \vdots \\ \mu_m & \mu_{m+1} & \cdots & \mu_{2m-1} \end{pmatrix}, \tag{16}$$

where m denotes the number of distinct eigenvalues of the non-linear eigenvalue problem (12) located in the interior of the closed curve γ. With these definitions, it can be shown [12] that the eigenvalues of the pencil $\mathsf{H}_m^< - \lambda\mathsf{H}_m$ are given by λ_i $(i = 1, ...m)$, where λ_i denotes the eigenvalue of the original non-linear eigenvalue problem (12).

Eigenvectors ψ_j of the original non-linear eigenvalue problem can be evaluated as follows:

$$\psi_j = [\mathsf{s}_0, \mathsf{s}_1, ..., \mathsf{s}_{m-1}]\, \mathsf{w}_j, \tag{17}$$

where w_j denotes the eigenvector of the pencil $\mathsf{H}_m^< - \lambda \mathsf{H}_m$, and s_j represents a vector defined as follows:

$$\mathsf{s}_j = \frac{1}{2\pi \mathrm{i}} \int_{z \in \gamma} z^j \mathsf{A}(z)^{-1} \mathsf{v} \mathrm{d}z. \tag{18}$$

In numerical analyses, we utilise random vectors for u and v in Eq. (13). Further, since we do not generally know the number of eigenvalues m in the closed curve γ in the complex plane, we estimate m by using the following procedure:

1. Compose the Hankel matrix H_M in Eq. (15) for a sufficiently large non-negative integer M.
2. Perform the singular value decomposition of H_M.
3. Set m as the number of the singular values of H_m larger than a sufficiently small $\delta > 0$.

When multiple eigenvalues exist in γ, the block version of the SS method is utilised. In the block version, the random vectors u and $\mathsf{v} \in \mathbb{C}^N$ shall be replaced with random matrices U and $\mathsf{V} \in \mathbb{C}^{N \times \ell}$, respectively, where ℓ denotes an integer larger than 1.

2.4. A fast direct solver with FMM representation

In the block version of the SS method, we need to evaluate $\mathsf{Y} := \mathsf{A}^{-1}(z)\mathsf{V}$ (see RHS of Eq. (13)) for $\mathsf{V} \in \mathbb{C}^{N \times \ell}$, which is equivalent to solving ℓ algebraic equations $\mathsf{A}(z)\mathsf{y}_i = \mathsf{v}_i$ $(i = 1, ..., \ell)$, where y_i and v_i denote the ith column of matrices Y and V, respectively. Due to the multiple right-hand sides, it is preferable to use a direct solver rather than an iterative solver to solve the algebraic equations. The conventional BEM combined with a direct linear solver cannot, however, be used effectively in the SS method due to its numerical cost. Hence, we need a "fast" direct solver. As possible candidates for the fast direct solver for algebraic equations stemming from boundary integral equations, we can mention the ID-based fast direct solvers [24], use of $\mathcal{H}$ matrix algebra with adaptive cross approximation (ACA) [25], etc. In this paper, we utilise a fast direct solver with the fast multipole representation [26], which shall henceforth be denoted as "direct FMM" in this paper. In the following subsections, we review the formulation of the direct FMM for standard (i.e., non-periodic) problems and present its extension for periodic problems.

2.4.1. The direct FMM for non-periodic problems

We first describe the formulation of the direct FMM for a non-periodic problem. To this end, we consider the following boundary value problem defined in a bounded domain Ω in $\mathbb{R}^2$:

$$\nabla^2 u(x) + \omega^2 \frac{\rho}{\mu} u(x) = 0, \quad x \in \Omega, \tag{19}$$

$$u(x) = \hat{u}, \quad x \in \Gamma_u, \tag{20}$$

$$q(x) := \frac{\partial u(x)}{\partial n} = \hat{q}, \quad x \in \Gamma_q, \tag{21}$$

where $\hat{\cdot}$ represents a known function. The boundary value problem can be translated into the following boundary integral equation:

$$c(x)u(x) + (\mathcal{D}_{\Gamma_q} u)(x) - (\mathcal{S}_{\Gamma_u} q)(x) = \hat{f}(x), \quad x \in \Gamma := \overline{\Gamma_u \cup \Gamma_q}, \tag{22}$$

where $\hat{f}(x) = (\mathcal{S}_{\Gamma_q} \hat{q})(x) - c(x)\hat{u}(x) - (\mathcal{D}_{\Gamma_u} \hat{u})(x)$ denotes a known function.

In the direct FMM, to solve the boundary integral equation (22) numerically, we first introduce a cell-quadtree structure that covers the entire boundary Γ (Figure 3) in the same way as the original FMM. We build a cube which circumscribes Γ and call this cube a cell of level 0. We then take a cell (a parent cell) of level ℓ ($\ell \geq 0$) and divide it into four equal sub-cubes whose edge length is half of that of the parent cell and call these sub-cubes cells (child cells) of level $\ell + 1$ if some collocation points of the boundary element belong to them. We continue to subdivide the cells unless the number of boundary elements belonging to the cell is smaller than a given number. A childless cell is called a leaf. We denote the ith cell in level ℓ and its centre as $C^{i,\ell}$ and $X^{i,\ell}$, respectively. Further, we denote the deepest level as L.

With these settings, Eq. (22) is evaluated with the following local expansion:

$$\hat{f}(x) = c(x)u(x) + (\mathcal{D}_{\Gamma_{\mathrm{N}i} \cap \Gamma_q} u)(x) - (\mathcal{S}_{\Gamma_{\mathrm{N}i} \cap \Gamma_u} q)(x) + \frac{\mathrm{i}}{4} \sum_{k=-\infty}^{\infty} I_k(\overrightarrow{X^{i,L}x}) L_{-k}(X^{i,L}), \quad x \in \Gamma^{i,L} := \Gamma \cap C^{i,L}, \tag{23}$$

where $C^{i,L}$ indicates a leaf cell to which x belongs. Further, $\Gamma_{\mathrm{N}i}$ denotes the part of the boundary which is defined as follows:

$$\Gamma_{\mathrm{N}i} = \bigcup_{j \in \mathcal{N}^{i,L}} \Gamma \cap C^{j,L}, \tag{24}$$

where $\mathcal{N}^{i,L}$ represents a set of cells which share at least one vertex with the cell $C^{i,L}$. Further, I_n in Eq. (23) denotes the incoming solution of the Helmholtz equation in $\mathbb{R}^2$ given as follows:

$$I_n(\overrightarrow{Ox}) = J_n\left(\omega \sqrt{\frac{\rho}{\mu}} r\right) e^{\mathrm{i}n\theta}, \tag{25}$$

where J_n denotes the Bessel function of order n, and (r, θ) represents the polar representation of $\overrightarrow{Ox}$. $L_k(X)$ in Eq. (23) indicates the coefficient of the local expansion defined as follows:

$$L_k(X^{i,\ell}) = \sum_{j \in \mathcal{I}^{i,\ell}} \left(\sum_{m=-\infty}^{\infty} O_{k-m}(\overrightarrow{X^{j,\ell} X^{i,\ell}}) M_m(X^{j,\ell}) \right) + \sum_{j \in \mathcal{P}^{i,\ell}} \left(\sum_{m=-\infty}^{\infty} I_{\ell-m}(\overrightarrow{X^{j,\ell-1} X^{i,\ell}}) L_m(X^{j,\ell}) \right), \tag{26}$$

for $\ell = 2, ..., L$, where $\mathcal{P}^{i,\ell}$ denotes a set of parent cells of $C^{i,\ell}$ and $\mathcal{I}^{i,\ell}$ represents called an interaction list of the cell $C^{i,\ell}$ defined as follows:

$$\mathcal{I}^{i,\ell} = \mathcal{N}^{p,\ell-1} \setminus \mathcal{N}^{i,\ell}, \tag{27}$$

where p denotes the index for the parent cell of $C^{i,\ell}$, i.e., $C^{p,\ell-1}$ represents the parent of $C^{i,\ell}$. O_n in Eq. (26) denotes the outgoing solution of the Helmholtz equation in $\mathbb{R}^2$ defined as follows:

$$O_n(\overrightarrow{Oy}) = H_n^{(1)}\left(\omega\sqrt{\frac{\rho}{\mu}}r\right)e^{in\theta}. \tag{28}$$

$M_m(X^{j,\ell})$ in Eq. (26) represents the multipole moment of the cell $C^{j,\ell}$ defined as follows:

$$M_m(X^{i,L}) = (-1)^m \int_{\Gamma^{i,L}\cup\Gamma_q} \frac{\partial I_m(\overrightarrow{X^{i,L}y})}{\partial n(y)} u(y)\mathrm{d}S(y) - (-1)^m \int_{\Gamma^{i,L}\cup\Gamma_u} I_m(\overrightarrow{X^{i,L}y})\frac{\partial u(y)}{\partial n}\mathrm{d}S(y) \quad \text{for leaf cell,} \tag{29}$$

$$M_m(X^{i,\ell}) = \sum_{j\in\mathcal{K}^{i,\ell}} \left(\sum_{m=-\infty}^{\infty} I_{\ell-m}(\overrightarrow{X^{j,\ell+1}X^{i,\ell}}) M_m(X^{j,\ell+1}) \right) \quad \text{for } 2 < \ell < L-1, \tag{30}$$

where $\mathcal{K}^{i,\ell}$ indicates a set of child cells of $C^{i,\ell}$. The formulae in the parentheses of the first (resp. second) term of RHS of Eq. (26) are called as the M2L (resp. L2L) formula and the formula in the parenthesis of the RHS of Eq. (30) is called as the M2M formula. In the numerical procedure,

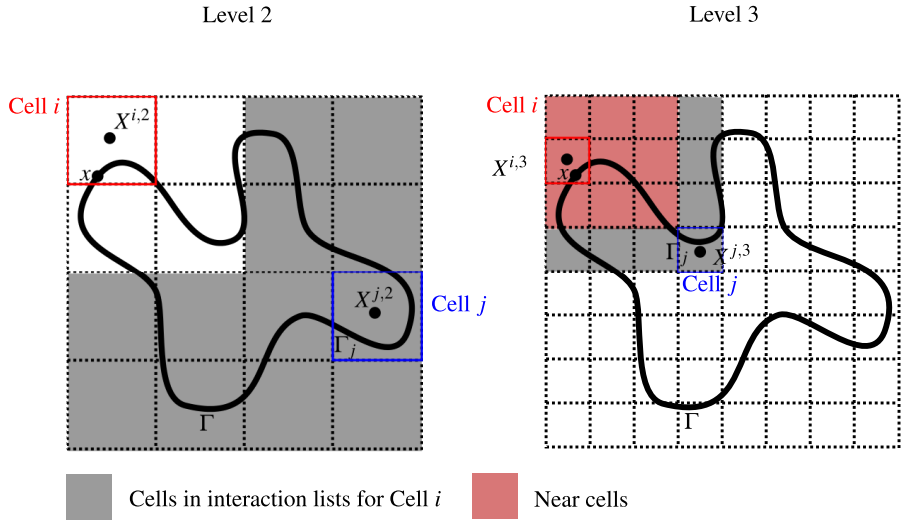

Figure 3: Quad tree. The deepest level is assumed here to be $L = 3$.

infinite series in Eqs. (23), (26) and (30) are truncated with $p < \infty$ terms. Note that $\hat{f}(x)$ in the RHS of Eq. (22) can also be evaluated with a similar procedure.

For the sake of reference, let us introduce the vector notations for Eqs. (23), (26), (29), and

(30) as follows:

$$\text{Local expansion} : \hat{\mathsf{f}}_i = \sum_{j \in \mathcal{N}^{i,L}} \mathsf{D}_{ij} \mathsf{z}_i + \mathsf{U}_i \mathsf{l}_i, \tag{31}$$

$$\text{M2L and L2L} : \mathsf{l}_i = \sum_{j \in \mathcal{I}^{i,\ell}} \mathsf{T}_{ij} \mathsf{m}_j + \sum_{j \in \mathcal{P}^{i,\ell}} \mathsf{R}_{ij} \mathsf{l}_j, \tag{32}$$

$$\text{Moment for leaf} : \mathsf{m}_i = \mathsf{V}_i \mathsf{z}_i, \tag{33}$$

$$\text{Moment for non leaf cells} : \mathsf{m}_i = \sum_{j \in \mathcal{K}^{i,\ell}} \mathsf{S}_{ij} \mathsf{m}_j, \tag{34}$$

where z_i denotes a set of u and q on the collocation points in the cell $C^{i,\ell}$, $\hat{\mathsf{f}}_i$ represents a set of $\hat{f}(x)$ in $C^{i,\ell}$, and $\mathsf{m}_i \in \mathbb{C}^{2p+1}$ indicates a vector containing the multipole moment in $C^{i,\ell}$ as follows:

$$\mathsf{m}_i = \left(M_{-p}(X^{i,\ell}), M_{-p+1}(X^{i,\ell}), \cdots, M_{-1}(X^{i,\ell}), M_0(X^{i,\ell}), M_1(X^{i,\ell}), \cdots, M_{p-1}(X^{i,\ell}), M_p(X^{i,\ell}) \right), \tag{35}$$

$\mathsf{l}_i \in \mathbb{C}^{2p+1}$ denotes a vector containing the coefficient of the local expansion defined similar to m_i. D_{ij}, T_{ij}, R_{ij}, V_i, and S_{ij} denote the relevant operators. Note that V_i in Eq. (33) is composed by discretising the boundary integral in Eq. (29) into the Gaussian quadrature.

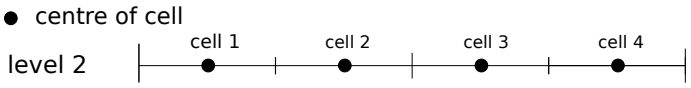

Figure 4: One-dimensional domain and its cell-tree structure.

In the original FMM [22, 23], the discretised version of Eq. (22) is solved with an iterative solver of algebraic equations such as GMRES, in which the matrix-vector product is carried out by the FMM. In the direct FMM, however, the set of equations (31), (32), (33), and (34) are solved using a direct solver, by letting l_i and m_i as well as z_i be the unknowns. Equation (36) shows a typical coefficient matrix for the direct FMM in the case of the one-dimensional problem (Figure 4):

$$\left[\begin{array}{cccc|cccc|cccc}
\mathsf{D}_{11} & \mathsf{D}_{12} & & & & & & \mathsf{U}_1 & & & & \\
\mathsf{D}_{21} & \mathsf{D}_{22} & \mathsf{D}_{23} & & & & \mathsf{U}_2 & & & & & \\
 & \mathsf{D}_{32} & \mathsf{D}_{33} & \mathsf{D}_{34} & & \mathsf{U}_3 & & & & & & \\
 & & \mathsf{D}_{43} & \mathsf{D}_{44} & \mathsf{U}_4 & & & & & & & \\
\hline
 & & & & -\mathsf{I} & & & & \mathsf{T}_{41} & \mathsf{T}_{42} & & \\
 & & & & & -\mathsf{I} & & & \mathsf{T}_{31} & & & \\
 & & & & & & -\mathsf{I} & & & & & \mathsf{T}_{24} \\
 & & & & & & & -\mathsf{I} & & & \mathsf{T}_{13} & \mathsf{T}_{14} \\
\hline
\mathsf{V}_1 & & & & & & & & -\mathsf{I} & & & \\
 & \mathsf{V}_2 & & & & & & & & -\mathsf{I} & & \\
 & & \mathsf{V}_3 & & & & & & & & -\mathsf{I} & \\
 & & & \mathsf{V}_4 & & & & & & & & -\mathsf{I}
\end{array}\right]
\left[\begin{array}{c}
\mathsf{z}_1 \\ \mathsf{z}_2 \\ \mathsf{z}_3 \\ \mathsf{z}_4 \\ \hline
\mathsf{l}_4 \\ \mathsf{l}_3 \\ \mathsf{l}_2 \\ \mathsf{l}_1 \\ \hline
\mathsf{m}_1 \\ \mathsf{m}_2 \\ \mathsf{m}_3 \\ \mathsf{m}_4
\end{array}\right]
=
\left[\begin{array}{c}
\hat{\mathsf{f}}_1 \\ \hat{\mathsf{f}}_2 \\ \hat{\mathsf{f}}_3 \\ \hat{\mathsf{f}}_4 \\ \hline
0 \\ 0 \\ 0 \\ 0 \\ \hline
0 \\ 0 \\ 0 \\ 0
\end{array}\right], \tag{36}$$

where the deepest level of the FMM is assumed to be $L = 2$. Since the coefficient matrix in Eq. (36) is sparse, the algebraic equation (36) is appropriately solved with a sparse direct solver

such as the PARDISO routine in the MKL library. Note that we have arranged the components of the matrix so as to reduce fill-ins in the direct solvers [26].

Since the size of the algebraic equation (36) is larger than that of the original equation, we consider approximating the off-diagonal blocks of the coefficient matrix in Eq. (36) with low rank matrices. To this end, we utilise the interpolative decomposition (ID) [27] to the M2L, M2M, and L2L operators. For the matrix in Eq. (36), we utilise the ID to blocks $\begin{bmatrix} \mathsf{T}_{41} \\ \mathsf{T}_{31} \end{bmatrix}$, $\begin{bmatrix} \mathsf{T}_{42} \end{bmatrix}$, $\begin{bmatrix} \mathsf{T}_{13} \end{bmatrix}$, and $\begin{bmatrix} \mathsf{T}_{24} \\ \mathsf{T}_{14} \end{bmatrix}$.

It is known that a rank-k matrix $\mathsf{A} \in \mathbb{C}^{m\times n}$ can be expressed in the following form:

$$\mathsf{A} = \widetilde{\mathsf{A}}\mathsf{V}^H, \tag{37}$$

where $\widetilde{\mathsf{A}} \in \mathbb{C}^{m\times k}$ denotes a sub-matrix of A, that is, $\widetilde{\mathsf{A}}$ is composed of k column vectors of A. By its definition, the reconstruction matrix $\mathsf{V}^H \in \mathbb{C}^{k\times n}$ contains the column-permutated identity $\mathsf{I} \in \mathbb{C}^{k\times k}$. It is also known that the ID (37) can be composed with a matrix V with entries not greater than 1. However, such V cannot be constructed in polynomial time. In this study, a variant of QR decomposition is used for composing the ID (37). Note that, in this case, the largest component of V is not necessarily less than 1. Since the rank k of matrix A is generally unknown, Eq. (37) is usually replaced with the following one:

$$\mathsf{A} = \widetilde{\mathsf{A}}\mathsf{V}^H + \mathsf{E}, \tag{38}$$

where $\mathsf{E} \in \mathbb{C}^{m\times n}$ denotes a matrix which represents an error for the ID. We can utilise a QR decomposition to determine $\widetilde{\mathsf{A}}$, V and k which satisfy $\|\mathsf{E}\| < \varepsilon_{\mathrm{ID}}$ with a preset tolerance $\varepsilon_{\mathrm{ID}}$. Note that the QR decomposition should carefully be performed to keep the orthogonality of the column vectors of Q [27].

The size of the algebraic equation (36) is reduced by the ID with the following procedure: $\mathsf{T}_1 = \begin{bmatrix} \mathsf{T}_{41} \\ \mathsf{T}_{31} \end{bmatrix}$ is, for example, low rank approximated with the ID as follows:

$$\mathsf{T}_1 = \widetilde{\mathsf{T}}_1\mathsf{F}_1^H, \tag{39}$$

where $\widetilde{\mathsf{T}}_1$ and F_1^H denote the sub-matrix of T_1 and reconstruction matrix for T_1, respectively. When the rank of $\mathsf{T} \in \mathbb{C}^{m\times n}$ is $k < \min\{m, n\}$, $\widetilde{\mathsf{T}}_1$ and F_1 are in $\mathbb{C}^{m\times k}$ and $\mathbb{C}^{k\times n}$, respectively. In order to replace T_1 in Eq. (36) with $\widetilde{\mathsf{T}}_1$, we need to replace m_1 with the following $\widetilde{\mathsf{m}}_1$:

$$\mathsf{T}_1\mathsf{m}_1 = \widetilde{\mathsf{T}}_1(\mathsf{F}_1^H\mathsf{m}_1) = \widetilde{\mathsf{T}}_1\widetilde{\mathsf{m}}_1, \tag{40}$$

where $\widetilde{\mathsf{m}}_1 = \mathsf{F}_1^H\mathsf{m}_1$ is in $\mathbb{C}^k$. In order to keep the coefficient matrix square, we need to replace V_1 with the following $\widetilde{\mathsf{V}}_1$:

$$\widetilde{\mathsf{V}}_1 = \mathsf{F}_1^H\mathsf{V}_1. \tag{41}$$

Thus, by applying the ID to T_1, the M2L block T_1 is column compressed, and the moment vector m_1 and the block V_1 are row compressed, which gives a smaller square coefficient matrix than the

original (36). $\begin{bmatrix} \mathsf{T}_{42} \end{bmatrix}$, $\begin{bmatrix} \mathsf{T}_{13} \end{bmatrix}$, $\begin{bmatrix} \mathsf{T}_{14} \\ \mathsf{T}_{24} \end{bmatrix}$ are column compressed in the same manner. After all the M2L coefficients are column compressed, Eq. (36) becomes as follows:

$$\left[\begin{array}{cccc|cccc|cccc} \mathsf{D}_{11} & \mathsf{D}_{12} & & & & & & \mathsf{U}_1 & & & & \\ \mathsf{D}_{21} & \mathsf{D}_{22} & \mathsf{D}_{23} & & & & \mathsf{U}_2 & & & & & \\ & \mathsf{D}_{32} & \mathsf{D}_{33} & \mathsf{D}_{34} & & \mathsf{U}_3 & & & & & & \\ & & \mathsf{D}_{43} & \mathsf{D}_{44} & \mathsf{U}_4 & & & & & & & \\ \hline & & & & -\mathsf{I} & & & & \widetilde{\mathsf{T}}_{41} & \widetilde{\mathsf{T}}_{42} & & \\ & & & & & -\mathsf{I} & & & \widetilde{\mathsf{T}}_{31} & & & \\ & & & & & & -\mathsf{I} & & & & & \widetilde{\mathsf{T}}_{24} \\ & & & & & & & -\mathsf{I} & & & \widetilde{\mathsf{T}}_{13} & \widetilde{\mathsf{T}}_{14} \\ \hline \widetilde{\mathsf{V}}_1 & & & & & & & & -\mathsf{I} & & & \\ & \widetilde{\mathsf{V}}_2 & & & & & & & & -\mathsf{I} & & \\ & & \widetilde{\mathsf{V}}_3 & & & & & & & & -\mathsf{I} & \\ & & & \widetilde{\mathsf{V}}_4 & & & & & & & & -\mathsf{I} \end{array}\right] \left[\begin{array}{c} \mathsf{z}_1 \\ \mathsf{z}_2 \\ \mathsf{z}_3 \\ \mathsf{z}_4 \\ \hline \mathsf{I}_4 \\ \mathsf{I}_3 \\ \mathsf{I}_2 \\ \mathsf{I}_1 \\ \hline \widetilde{\mathsf{m}}_1 \\ \widetilde{\mathsf{m}}_2 \\ \widetilde{\mathsf{m}}_3 \\ \widetilde{\mathsf{m}}_4 \end{array}\right] = \left[\begin{array}{c} \hat{\mathsf{f}}_1 \\ \hat{\mathsf{f}}_2 \\ \hat{\mathsf{f}}_3 \\ \hat{\mathsf{f}}_4 \\ \hline 0 \\ 0 \\ 0 \\ 0 \\ \hline 0 \\ 0 \\ 0 \\ 0 \end{array}\right]. \tag{42}$$

The coefficient matrix in Eq. (42) can further be compressed by compressing $\begin{bmatrix} \widetilde{\mathsf{T}}_{41} & \widetilde{\mathsf{T}}_{42} \end{bmatrix}$, $\begin{bmatrix} \widetilde{\mathsf{T}}_{31} \end{bmatrix}$, $\begin{bmatrix} \widetilde{\mathsf{T}}_{24} \end{bmatrix}$ and $\begin{bmatrix} \widetilde{\mathsf{T}}_{13} & \widetilde{\mathsf{T}}_{14} \end{bmatrix}$ in a row, which can be carried out by applying the ID to the transposed matrices. Let us assume that the rank of $\begin{bmatrix} \widetilde{\mathsf{T}}_{13} & \widetilde{\mathsf{T}}_{14} \end{bmatrix} \in \mathbb{C}^{m\times n}$ is $k < \min\{m, n\}$. Then, $\begin{bmatrix} \widetilde{\mathsf{T}}_{13} & \widetilde{\mathsf{T}}_{14} \end{bmatrix} \in \mathbb{C}^{m\times n}$ is row compressed as follows:

$$\begin{bmatrix} \widetilde{\mathsf{T}}_{13} & \widetilde{\mathsf{T}}_{14} \end{bmatrix} = \mathsf{E}_1 \begin{bmatrix} \hat{\mathsf{T}}_{13} & \hat{\mathsf{T}}_{14} \end{bmatrix}, \tag{43}$$

where $\mathsf{E}_1 \in \mathsf{C}^{m\times k}$ and $\begin{bmatrix} \hat{\mathsf{T}}_{13} & \hat{\mathsf{T}}_{14} \end{bmatrix} \in \mathsf{C}^{k\times n}$ denote the row-compression counterparts for F_1 and $\widetilde{\mathsf{T}}_1$, respectively. With these definitions, we replace $\begin{bmatrix} \widetilde{\mathsf{T}}_{13} & \widetilde{\mathsf{T}}_{14} \end{bmatrix}$, I_1 and U_1 with $\begin{bmatrix} \hat{\mathsf{T}}_{13} & \hat{\mathsf{T}}_{14} \end{bmatrix}$, $\hat{\mathsf{I}}_1 = \hat{\mathsf{T}}_{13}\widetilde{\mathsf{m}}_3 + \hat{\mathsf{T}}_{14}\widetilde{\mathsf{m}}_4$ and $\hat{\mathsf{U}}_1 = \mathsf{U}_1\mathsf{E}_1$, respectively.

Note that, in the case that the multi-level FMM is utilised, i.e., $L \geq 3$, M2M and L2L coefficients are compressed along with the M2L coefficient; this procedure can be found in the original paper [26].

2.5. Direct FMM for periodic problems

In this subsection, we modify the direct FMM for periodic problems. We are now interested in solving the following boundary integral equation defined on $x \in \Gamma$:

$$c(x)u(x) + (\mathcal{D}_{\Gamma_q}u)(x) + \sum_{k=1}^{2}(\mathcal{D}_{\Gamma_{\mathrm{I}k}}u)(x) + \sum_{k=1}^{2}(\widetilde{\mathcal{D}}_{\Gamma_{\mathrm{D}k}}u)(x) - (\mathcal{S}_{\Gamma_u}q)(x) - \sum_{k=1}^{2}(\mathcal{S}_{\Gamma_{\mathrm{I}k}}q)(x) + \sum_{k=1}^{2}(\widetilde{\mathcal{S}}_{\Gamma_{\mathrm{D}k}}q)(x) = \hat{f}(x), \tag{44}$$

where $\hat{f}(x)$ denotes a known function.

In order to solve the integral equation (44) with the direct FMM, we need to modify the local expansion (23) and the moment for leaf cells (29) as follows:

$$\begin{aligned}\hat{f}(x) = c(x)u(x) + (\mathcal{D}_{\Gamma_{\mathrm{N}i}\cap\Gamma_q}u)(x) + \sum_{k=1}^{2}\left(\mathcal{D}_{\Gamma_{\mathrm{N}i}\cap\Gamma_{\mathrm{I}k}}u\right)(x) + \sum_{k=1}^{2}\left(\mathcal{D}_{\Gamma_{\mathrm{N}i}\cap\Gamma_{\mathrm{D}k}}u\right)(x)\\ - (\mathcal{S}_{\Gamma_{\mathrm{N}i}\cap\Gamma_u}q)(x) - \sum_{k=1}^{2}\left(\mathcal{S}_{\Gamma_{\mathrm{N}i}\cap\Gamma_{\mathrm{I}k}}q\right)(x) + \sum_{k=1}^{2}\left(\mathcal{S}_{\Gamma_{\mathrm{N}i}\cap\Gamma_{\mathrm{D}k}}q\right)(x)\\ + \frac{\mathrm{i}}{4}\sum_{k=-\infty}^{\infty} I_k(\overrightarrow{X^{i,L}x})L_{-k}(X^{i,L}) \quad x\in\Gamma^{i,L} := \Gamma\cap C^{i,L},\end{aligned} \tag{45}$$

$$\begin{aligned}M_m(X^{i,L}) = (-1)^m\int_{\Gamma^{i,L}\cap(\Gamma_q\cup\Gamma_{\mathrm{I}})}\frac{\partial I_m(\overrightarrow{X^{i,L}y})}{\partial n(y)}u(y)\mathrm{d}S(y) - (-1)^m\int_{\Gamma^{i,L}\cap(\Gamma_u\cup\Gamma_{\mathrm{I}})} I_m(\overrightarrow{X^{i,L}y})\frac{\partial u(y)}{\partial n}\mathrm{d}S(y)\\ + \sum_{k=1}^{2}(-1)^m\int_{\Gamma^{i,L}\cap(\Gamma_q\cup\Gamma_{\mathrm{D}k})}\frac{\partial I_m(\overrightarrow{X^{i,L}y})}{\partial n(y)}\exp(\mathrm{i}k\cdot a_k)u(y-a_k)\mathrm{d}S(y)\\ + \sum_{k=1}^{2}(-1)^m\int_{\Gamma^{i,L}\cap(\Gamma_u\cup\Gamma_{\mathrm{D}k})} I_m(\overrightarrow{X^{i,L}y})\exp(\mathrm{i}k\cdot a_k)\frac{\partial u(y-a_k)}{\partial n}\mathrm{d}S(y).\end{aligned} \tag{46}$$

The rest of the formulae such as M2L, L2L and M2M are the same as those for the non-periodic problem; see Eqs. (26) and (30). With these modifications, the algebraic equation in the direct FMM for one-dimensional problem in Eq. (36) becomes as follows:

$$\left[\begin{array}{cccc|cccc|cccc}
\mathsf{D}_{11} & \mathsf{D}_{12} & & \mathsf{S}_{11} & & & & \mathsf{U}_1 & & & & \\
\mathsf{D}_{21} & \mathsf{D}_{22} & \mathsf{D}_{23} & \mathsf{S}_{21} & & & \mathsf{U}_2 & & & & & \\
\widetilde{\mathsf{D}}_{31} & \mathsf{D}_{32} & \mathsf{D}_{33} & \widetilde{\mathsf{A}}_{34} & & \mathsf{U}_3 & & & & & & \\
\widetilde{\mathsf{D}}_{41} & & \mathsf{D}_{43} & \widetilde{\mathsf{A}}_{44} & \mathsf{U}_4 & & & & & & & \\
\hline
 & & & & -\mathsf{I} & & & & \mathsf{T}_{41} & \mathsf{T}_{42} & & \\
 & & & & & -\mathsf{I} & & & \mathsf{T}_{31} & & & \\
 & & & & & & -\mathsf{I} & & & & & \mathsf{T}_{24} \\
 & & & & & & & -\mathsf{I} & & & \mathsf{T}_{13} & \mathsf{T}_{14} \\
\hline
\mathsf{V}_1 & & & \overline{\mathsf{V}}_1 & & & & & -\mathsf{I} & & & \\
 & \mathsf{V}_2 & & & & & & & & -\mathsf{I} & & \\
 & & \mathsf{V}_3 & & & & & & & & -\mathsf{I} & \\
\widetilde{\mathsf{V}}_4 & & & \widetilde{\overline{\mathsf{V}}}_4 & & & & & & & & -\mathsf{I}
\end{array}\right]\left[\begin{array}{c}\mathsf{z}_1\\ \mathsf{z}_2\\ \mathsf{z}_3\\ \mathsf{z}_4\\ \hline \mathsf{l}_4\\ \mathsf{l}_3\\ \mathsf{l}_2\\ \mathsf{l}_1\\ \hline \mathsf{m}_1\\ \mathsf{m}_2\\ \mathsf{m}_3\\ \mathsf{m}_4\end{array}\right] = \left[\begin{array}{c}\hat{\mathsf{f}}_1\\ \hat{\mathsf{f}}_2\\ \hat{\mathsf{f}}_3\\ \hat{\mathsf{f}}_4\\ \hline 0\\ 0\\ 0\\ 0\\ \hline 0\\ 0\\ 0\\ 0\end{array}\right], \tag{47}$$

where it is assumed that cell 1 (resp. 4) contains Γ_{I} (resp. Γ_{D}); z_1 and z_4 consist of u on $(\Gamma_q\cap\Gamma^{1,L})\cup\Gamma_{\mathrm{I}}$ and q on $(\Gamma_u\cap\Gamma^{1,L})\cup\Gamma_{\mathrm{I}}$, respectively. Further, S_{i1}, $\widetilde{\mathsf{A}}_{i1}$, $\widetilde{\mathsf{B}}_{i4}$, $\overline{\mathsf{V}}_1$, $\widetilde{\mathsf{V}}_4$, and $\widetilde{\overline{\mathsf{V}}}_4$ represent

matrices stemming from the following operators:

$$(\mathcal{S}_{i1}q)(x) = -\int_{\Gamma_1\cap\Gamma^{i,L}} G(x-y)q(y)\mathrm{d}S(y) \quad x\in\Gamma^{i,L}, \tag{48}$$

$$(\widetilde{\mathcal{D}}_{i1}u)(x) = \int_{\Gamma_{\mathrm{D}}\cap\Gamma^{i,L}} \frac{\partial G(x-y)}{\partial n(y)}\exp(\mathsf{i}\mathsf{k}\cdot a_1)u(y-a_1)\mathrm{d}S(y) \quad x\in\Gamma^{i,L}, \tag{49}$$

$$\begin{aligned}(\widetilde{\mathcal{A}}_{i4}z)(x) = &-\int_{\Gamma_u\cap\Gamma^{4,L}} G(x-y)q(y)\mathrm{d}S(y) + \int_{\Gamma_q\cap\Gamma^{4,L}} \frac{\partial G(x-y)}{\partial n(y)}u(y)\mathrm{d}S(y),\\ &+\int_{\Gamma_{\mathrm{D}}} G(x-y)\exp(\mathsf{i}\mathsf{k}\cdot a_1)q(y-a_i)\mathrm{d}S(y) \quad x\in\Gamma^{i,L},\end{aligned} \tag{50}$$

$$(\overline{\mathcal{V}}_1q)(X^{1,L}) = -(-1)^m\int_{\Gamma_1\cap\Gamma^{1,L}} I_m(\overrightarrow{X^{1,L}y})q(y)\mathrm{d}S(y) \quad m=-p,-p+1,\cdots,0,\cdots,p-1,p, \tag{51}$$

$$(\widetilde{\mathcal{V}}_4u)(X^{4,L}) = (-1)^m\int_{\Gamma_{\mathrm{D}}\cap\Gamma^{4,L}} \frac{\partial I_m(\overrightarrow{X^{4,L}y})}{\partial n(y)}\exp(\mathsf{i}\mathsf{k}\cdot a_1)u(y-a_1)\mathrm{d}S(y) \quad m=-p,-p+1,\cdots,0,\cdots,p-1,p, \tag{52}$$

$$(\widetilde{\overline{\mathcal{V}}}_4q)(X^{4,L}) = -(-1)^m\int_{\Gamma_{\mathrm{D}}\cap\Gamma^{4,L}} I_m(\overrightarrow{X^{4,L}y})\exp(\mathsf{i}\mathsf{k}\cdot a_1)q(y-a_1)\mathrm{d}S(y) \quad m=-p,-p+1,\cdots,0,\cdots,p-1,p. \tag{53}$$

We have allocated u on Γ_I and q on Γ_I in (47) to where z on Γ_I and z on Γ_D are allocated in (36), respectively. It is, however, that the arrangement of the unknowns may affect the performance of the sparse direct solver, which may be addressed in our future publications.

A low-rank approximation procedure for the M2L blocks T_{ij} in Eq. (47) (and M2M/L2L blocks for the case of $L > 2$) can be performed in a manner similar to that of non-periodic problems.

2.6. Fictitious eigenfrequency

The present formulation may provide some non-physical eigenvalues which are so called fictitious (or irregular) eigenvalues [21, 28]. The irregular frequency detected by the present method can be removed with the following procedure:

- Eigenvalues detected independently of the Bloch wave vector may correspond to fictitious eigenvalues.
  Since the fictitious eigenvalue corresponds to an eigenfrequency of an interior domain formed by a closed curve Γ_{B} in the unit cell, the irregular frequency appears independently of the Bloch wave vector.

- Use of the Burton-Miller method.
  The irregular eigenvalues calculated with different coupling constants in the Burton-Miller method are different from each other, while the physical eigenvalues are not affected by the coupling constant. We note that, although it is well known that the Burton-Miller integral equation is well posed provided that the imaginary part of the coupling constant is non-zero, it is only true for real frequency ω [29]. By using the Burton-Miller method, we can shift a (real-valued) fictitious eigenvalue to a complex number with non-zero imaginary parts.

Note that, in the following examples, we have not used the above procedure to remove the fictitious eigenvalues since the present method does not detected any irregular frequency. This is because that the domain Ω for Section 3.1 does not include Γ_{B} and explored frequency range for Section 3.2 is extremely low.

2.7. Numerical apparatus

In the numerical experiments, the integral path γ in Eq. (14) is assumed to be a circle and the counter integral is evaluated with the N_{t}-point trapezoidal rule [12]. Our algorithm is summarised as follows:

for i_{t}=0 to $N_{\mathrm{t}} - 1$ **do**
  (precomputation) Set $\omega_{i_{\mathrm{t}}} \leftarrow \gamma_{\mathrm{c}} + \gamma_{\mathrm{r}} \exp(2\pi \mathrm{i}(i_{\mathrm{t}} + 1/2)/N_{\mathrm{t}})$, where γ_{c} and γ_{r} are the centre and the radius of the integral path γ of the moment in Eq. (14), respectively.
  (precomputation) Precompute some parts of the matrices which are common to all k in Eq. (47). Near-field interactions on Γ_{B}, coefficients of M2L, L2L and M2M, and the coefficient of the local expansion can be precomputed outside the loop over k.
end for
for Wave vectors on the reduced Brillouin zone **do**
  for $j = 0$ to $2M - 1$, where M denotes a sufficiently large integer. **do**
    1. initialise $\mu_j = 0$
  end for
  for i_{t}=0 to $N_{\mathrm{t}} - 1$ **do**
    2. Set $\omega_{i_{\mathrm{t}}} \leftarrow \gamma_{\mathrm{c}} + \gamma_{\mathrm{r}} \exp(2\pi \mathrm{i}(i_{\mathrm{t}} + 1/2)/N_{\mathrm{t}})$.
    3. Solve $\mathsf{A}(\omega_{i_{\mathrm{t}}})\mathsf{y} = \mathsf{v}$ by the direct FMM, where $\mathsf{A} \in \mathbb{C}^{N \times N}$ denotes the influence coefficient in Eq. (12) associated with the integral operators in Eqs. (7)–(10), N represents the number of boundary elements, and $\mathsf{v} \in \mathbb{C}^n$ indicates a random vector.
    for $j = 0$ to $2M - 1$ **do**
      4. $\mathsf{s}_j \leftarrow \mathsf{s}_j + \frac{\omega_{i_{\mathrm{t}}} - \gamma_{\mathrm{c}}}{\gamma_{\mathrm{r}}} \mathsf{y}$, see Eq. (18).
    end for
  end for
  for $j = 0$ to $2M - 1$ **do**
    5. The moment μ_j in Eq. (14) is evaluated as $\mu_j = \mathsf{u}^H \mathsf{s}_j$.
  end for
  6. Construct H_M in Eq. (15)
  7. Find the singular values σ_i ($i = 1, ..., M$) of H_M and the largest integer m such that $\sigma_m > \delta$, where σ_m denotes the mth largest singular value of H_M.
  8. Construct H_m in Eq. (15) and $\mathsf{H}_m^<$ in Eq. (16) and find the eigenvalues λ_j ($j = 1, ..., m$) of the pencil $\mathsf{H}_m - \lambda \mathsf{H}_m^<$.
  9. The eigenvalues of the original non-linear eigenvalue problem are obtained as $z_j = \gamma_{\mathrm{c}} + \gamma_{\mathrm{r}} \lambda_j$.
  10. The eigenvectors $u(x)$ for $x \in \Gamma$ are obtained by Eq. (17). When the whole distribution of u in Ω is needed, the inner point calculation is required.
end for

When the block version of the SS method is used, the random vectors u and v are replaced with random matrices U and $\mathsf{V} \in \mathbb{C}^{N \times \ell}$, respectively.

3. Numerical examples

In this section, we present some numerical examples to confirm the validity and the efficiency of the proposed method. We first state common issues to all the examples to follow:

- Period L_i $(i = 1, 2)$ is normalised as $L_i = 1.0$.
- The density ρ and the shear modulus μ are normalised as $\rho = 1$ and $\mu = 1$, respectively.
- The number of wave vectors on the edge of the reduced first Brillouin zone: 21.
- The number of integration points for the trapezoidal rule on the integral path γ: $N_{\mathrm{t}} = 256$.
- The number of columns of the random matrices U and V for the block SS method: 6
- Hankel matrices H_M in (15) are initially calculated for $M = 8$.
- The deepest level of the FMM-tree is determined by numerical experiments.
- The infinite series in (26), (30) are truncated with $p = \max\{|\sqrt{\varepsilon}\omega_{i_{\mathrm{t}}}|L_{\mathrm{c}} + 3\log(|\sqrt{\varepsilon}\omega_{i_{\mathrm{t}}}|L_{\mathrm{c}} + \pi),\ 20\}$, where L_{c} denotes the length of the edge of cell in level 2 (=0.25) [30].
- All numerical experiments were run on a PC with Intel Xeon CPU E5-2640 v3 with 16 cores. The code is OpenMP parallelised.
- The computational time is measured using the OpenMP run-time library routine `omp_get_wtime`, and the computational time includes the time for the precomputation in the algorithm presented in Section 2.6.

In some of the following examples, we have compared the performance of the proposed method with that of a conventional-BEM-based eigensolver combined with the SS method. In the implementation of the conventional BEM, we have precomputed coefficient matrices for single- and double- layer potentials for all the sampling points $\omega_{i_{\mathrm{t}}}$.

3.1. Infinite domain

We first consider the infinite domain $\mathbb{R}^2$, which is considered to be the simplest periodic domain with an arbitrary period L_i $(i = 1, 2)$. With this example, we can check the accuracy of the proposed methodology since the analytical solution for the eigenvalues is available [31]. The analytical solution is obtained as

$$|\mathsf{k} + 2\pi(n, m)^t|, \tag{54}$$

where n and m are integers.

Figure 5 shows the band structure for $0.1 \leq \omega \leq 10.1$ obtained with the present method and the analytical method. For the present method, the periodic boundaries Γ_{I} and Γ_{D} are divided into $N = 320$ boundary elements. Further, the integral path γ in the complex plane for the moments in Eq. (14) is set as circles whose radius and centre are 1.0 and $1.1 + 2.0 \times n + 0\mathrm{i}$, $(n = 0, 1, 2, 3, 4, 5)$,

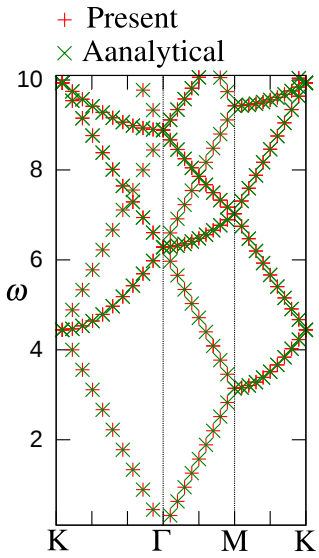

Figure 5: Band structure for the infinite domain $\mathbb{R}^2$.

respectively. The tolerance $\varepsilon_{\mathrm{ID}}$ for the ID is set as $\varepsilon_{\mathrm{ID}} = 10^{-12}$. One observes that the results of the present method agree well with those of the analytical method, from which the validity of the proposed method is confirmed.

We next investigate how the accuracy of the eigenvalues is affected by the quality of the boundary element mesh and the tolerance for the ID. To this end, we have computed the eigenvalues by varying the number of boundary elements N and the tolerance $\varepsilon_{\mathrm{ID}}$ for the ID. For this experiment, we selected $\mathsf{k} = (\pi/2, 0)^t$ as the wave vector with which nine eigenvalues exist in the frequency range of $0.1 \leq \omega \leq 10.1$. Table 1 shows the number of the eigenvalues found by the present SS method for various pairs of $(N, \varepsilon_{\mathrm{ID}})$, which indicates that the present method can find correct eigenvalues in the case of $N \geq 80$ and $\varepsilon_{\mathrm{ID}} \leq 10^{-10}$. Note that, in the case of $N = 80$ and $\omega = 10.1$, the number of boundary elements per wave is $40\pi/10.1 \simeq 12.442$.

Table 1: The number of eigenvalues found by the present method for the Bloch wave vector $\mathsf{k} = (\pi/2, 0)^t$ (The actual number of the eigenvalue is 9).

	$\varepsilon = 10^{-9}$	10^{-10}	10^{-11}	10^{-12}	10^{-13}	10^{-14}	10^{-15}	10^{-16}
$N = 40$	7	7	7	7	7	7	7	7
$N = 80$	9	9	9	9	9	9	9	9
$N = 160$	9	9	9	9	9	9	9	9
$N = 320$	10	9	9	9	9	9	9	9
$N = 640$	9	9	9	9	9	9	9	9
$N = 1280$	9	9	9	9	9	9	9	9
$N = 2560$	10	9	9	9	9	9	9	9

We then investigate the asymptotic behaviour of the accuracy of the present method with re-

spect to the number of boundary elements N. Figure 6 (left) shows the relative ℓ_2-error of the eigenvalues for $\mathsf{k} = (\pi/2, 0)^t$ against the number of boundary elements N_{BEM} for the case of $\varepsilon = 10^{-10}$. One may observe that the numerical error of the present method scales as $O(N_{\mathrm{BEM}}^{-1})$, which is reasonable since the constant elements are used in the boundary element analysis. For comparison, we have also plotted the relative ℓ_2-error of the finite-element results in Figure 6 (right). In the implementation of the FEM, although the hp-FEM can achieve exponential convergence as indicated in [6], we have used standard triangular linear elements. This is because we would like to compare the performance of the proposed solver with a standard and widely used one. The quasi-periodic boundary conditions (4) and (5) are regarded as the essential boundary condition in composing the finite element equations. The finite element matrices which are common to k are precomputed and stored in LAPACK band form. The resulting generalised eigenvalue problem is solved by ARPACK routines in which the matrix-vector products are parallelised by OpenMP. One may observe that the numerical error of the FEM scales as $O(N_{\mathrm{FEM}}^{-1})$. Since the DoFs for the

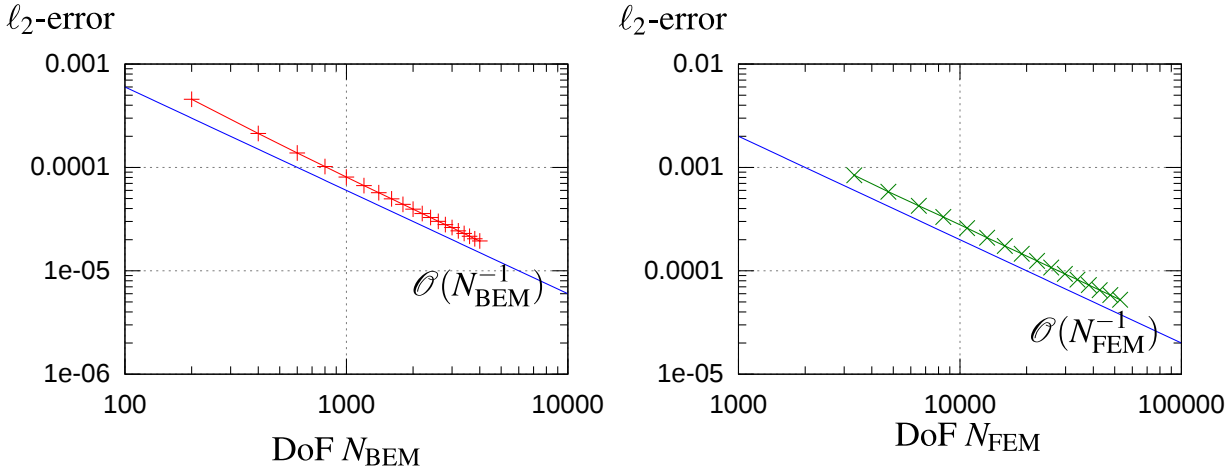

Figure 6: ℓ_2-error of the eigenvalues of $\mathbb{R}^2$ for $\mathsf{k} = (\pi/2, 0)^t$ obtained by (left:) the proposed method (right:) a FEM. The horizontal axis represents DoF for each method. In the calculation by the proposed method, $\varepsilon_{\mathrm{ID}} = 10^{-10}$ is used as the tolerance of ID.

present method and the FEM are quite different, we show the ℓ_2-error against the actual computational time in Figure 7. We have confirmed that the error of the present method is smaller than that of the FEM provided that the computational time is the same. We have also confirmed that ARPACK routine sometimes takes unexpectedly large number of iterations to find eigenvalues in Figure 7. This is because ARPACK uses a random vector as the initial guess for Arnoldi bases. We would therefore conclude that the present SS method is more stable than ARPACK routines.

With these observations, we conclude that the present methodology can appropriately solve the eigenvalue problem stemming from the periodic problems.

3.2. Periodic array of split-ring resonators

We next consider a doubly periodic array of split-ring resonators (SRR) [32] in Figure 8, with which the homogeneous Neumann boundary condition is imposed on Γ_{B}. For this example, we

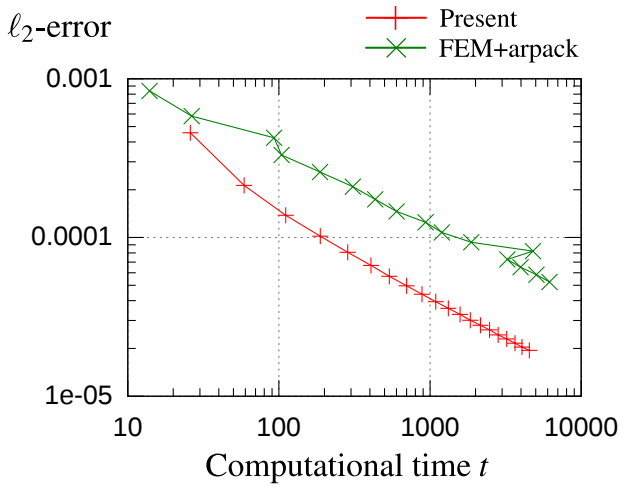

Figure 7: ℓ_2-error of the eigenvalues by the present and the FEM vs. the actual computational time.

used $N = 520$ boundary elements: 320 for the boundaries of the split-ring resonator Γ_B and 200 for those of the periodic boundaries $\Gamma_I \cup \Gamma_D$. The centre γ_c and radius γ_r of the counter integral path γ is set as $(\gamma_c, \gamma_r) = (2.0 + 0i, 2.0)$, that is, the band structure for $0 \leq \omega \leq 4.0$ is calculated.

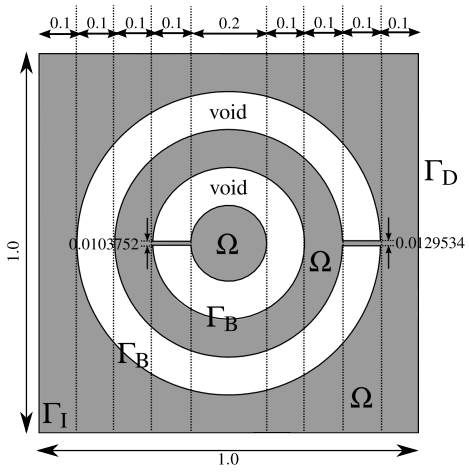

Figure 8: Split-ring resonator.

The obtained band diagram shown in Figure 9 agreed well with the reference [32], with which we confirm the validity of the proposed methodology for a relatively complicated geometry.

We next discuss the timing of the proposed method. Table 2 shows the computational time required to compute the band diagram shown in Figure 9 versus the number of boundary elements N with different ε_{ID}. While the computational time with the conventional BEM scales as $O(N^2)$, that of the proposed method scales as $O(N \log^2 N)$ for $N < 1000$. Although, for larger N, the proposed method seems to fail to achieve $O(N \log^\alpha N)$ computational complexity with small $\alpha > 0$, the proposed method is considerably faster than the conventional BEM. Further, one observes that

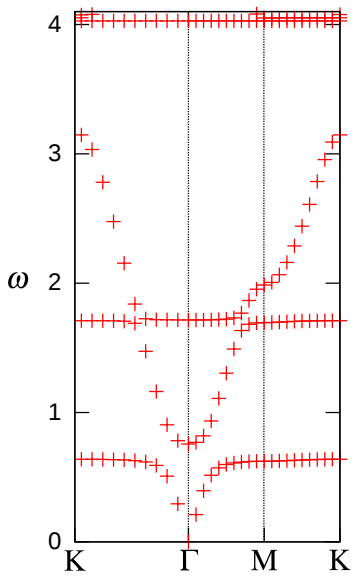

Figure 9: Band diagram for the split ring resonator obtained with $\varepsilon_{\mathrm{ID}} = 1.0 \times 10^{-12}$.

the proposed method is faster than the conventional BEM when N is larger than several thousands. With these observations, we conclude that the proposed methodology is effective, at least for moderate size problems in a two-dimensional domain. For larger and/or three dimensional problems, the direct FMM can be replaced with other fast direct solvers [24, 25], which will be addressed in our future publications. As shown in Table 2, when a larger tolerance $\varepsilon_{\mathrm{ID}}$ is utilised, the computational time is slightly reduced. This is because the size of the coefficient matrix for the direct FMM is reduced when the larger tolerance is utilised (see Eq. (42)). We note, however, if the tolerance is larger than 1.0×10^{-10}, the proposed method tends to find spurious (or non-physical) eigenvalues and/or fails to find the correct eigenvalues (Figure 10), which is consistent with the discussion in Section 3.1.

Table 2: Computational time for calculation of band structure for periodic array of SRR.

The number of boundary elements N	208	530	1060	2080	4270
Proposed ($\varepsilon_{\mathrm{ID}} = 1.0 \times 10^{-12}$)	150.1	257.6	530.8	1585.0	6287.2
Proposed ($\varepsilon_{\mathrm{ID}} = 1.0 \times 10^{-16}$)	220.1	317.7	605.3	1619.9	6340.5
Conventional BEM	7.1	61.1	268.0	1268.2	7956.2

Figure 11 shows the eigenvectors for the Bloch vector $\mathsf{k} = (\pi\ , pi)^t$. The eigenvector u is normalised as $\|u\|_{L^2(\Omega)} = 1$. As shown in the figure, the proposed methodology can provide not only eigenvalues but also eigenvectors.

As indicated in Eqs. (36) and (47), the number of non-zeros in the coefficient matrix increases in the case of periodic problems. This is because the near-interaction and the operation for moments for leaf cells are modified as Eqs. (45) and (46), respectively. Thus, we investigate how the computational cost is affected by the increase in the number of non-zeros. To this end, we compare the number of non-zero components of the coefficient matrix in the algebraic equations

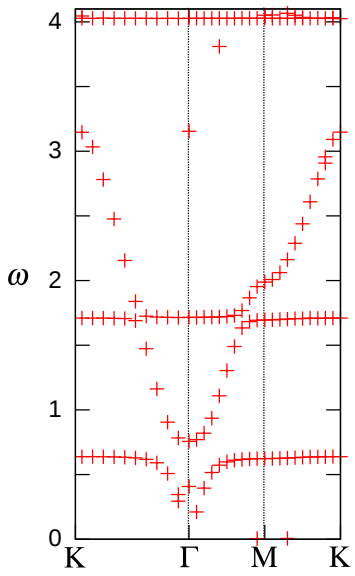

Figure 10: Band diagram obtained with $\varepsilon_{\mathrm{ID}} = 1.0 \times 10^{-4}$. Spurious solutions are plotted.

for the periodic problem with that for a non-periodic problem. As a non-periodic problem, we consider the SRR (Figure 8) whose periodic boundary condition on $\Gamma_{\mathrm{I}} \cup \Gamma_{\mathrm{D}}$ is replaced by the homogeneous Neumann one. We set the angular frequency as $\omega = 4.00 + 0.02\mathrm{i}$ for both periodic and non-periodic problems and solved the algebraic equations for six random right-hand sides. The boundaries $\Gamma_{\mathrm{I}} \cup \Gamma_{\mathrm{D}} \cup \Gamma_{\mathrm{B}}$ are divided into 2130 boundary elements. Further, the Bloch wave vector $k = (0, 0)$ is used for the periodic problem. Figure 12 shows the non-zero pattern for a part of the coefficient matrices in Eq. (36) and (47) which corresponds to near-interactions (upper-left part of the matrices). One observes that the columns corresponding to $\Gamma_{\mathrm{I}} \cup \Gamma_{\mathrm{D}}$ becomes dense when the periodic problem is considered. Table 3 shows the number of non-zeros and the computational time for both problems. Although the number of non-zeros increases for the periodic problem, the computational time for the periodic problem is almost the same as that for the non-periodic problem. Hence, we conclude that the periodic problem can appropriately be solved with the present formulation. The non-zeros can be reduced when the Green function [10] which satisfies the periodic boundary conditions (4) and (5) is utilised.

Table 3: Non-zeros and computational time

	#near-interactions	#coef. of moments	#total non-zeros	computational time (sec)
Periodic	2,322,698	91,852	2,635,998	25.568
Non-periodic	1,788,148	67,052	2,076,648	24.493

4. Concluding remarks

We have proposed a numerical method for bandgap calculations related to two dimensional periodic problems with the SS method and a fast direct BEM. We have modified the direct FMM

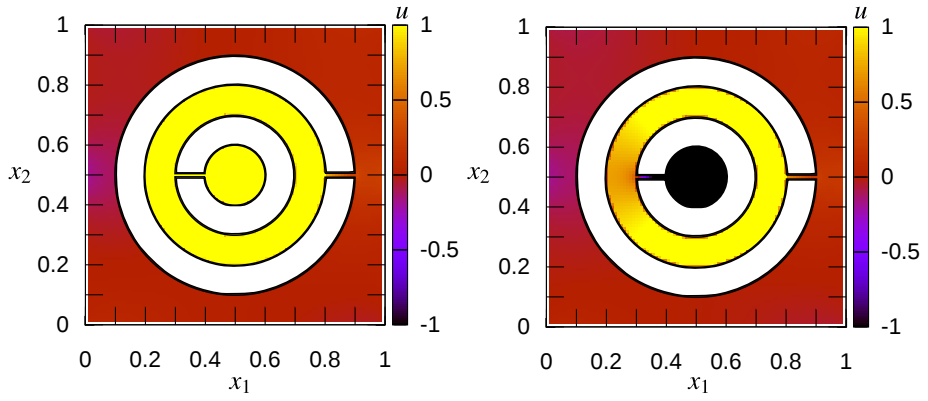

Figure 11: Eigenvectors for the periodic array of circular holes for the Bloch wave vector $\mathsf{k} = (\pi,\ \pi)^t$. Left and right figure correspond to the eigenvalue $\omega = 0.806,$ and 1.817, respectively.

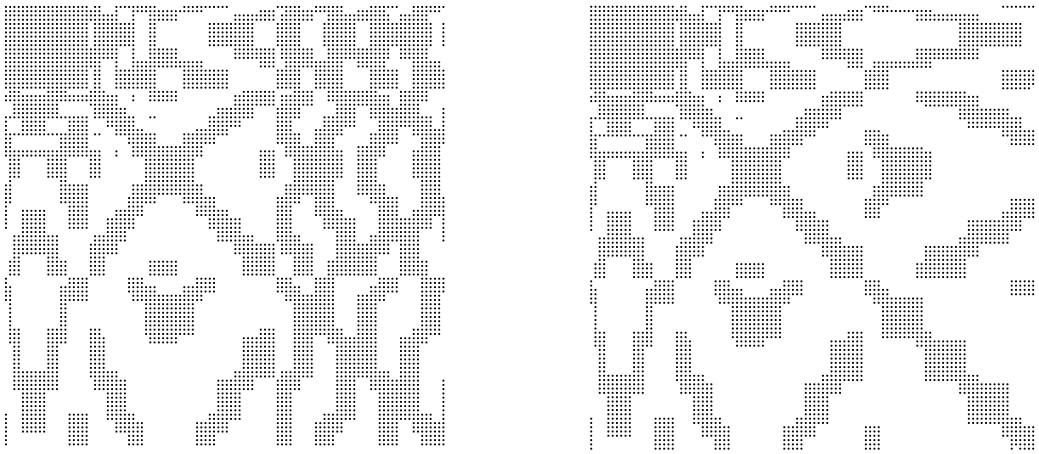

Figure 12: Non-zero component in near-interactions for (left:) periodic problem, (right:) non-periodic problem.

proposed by Pals [26] to deal with the periodic problems, and installed the direct FMM into the algorithm of the SS method. Through numerical experiments, we have confirmed that the accuracy of the proposed method with appropriate parameters is sufficient for engineering applications, and the computational cost of the proposed method is lower than that of a conventional FEM.

In our future work, we plan to investigate the use of other fast direct solvers [24, 25] in the algorithm of the SS method to enhance the applicability of the proposed eigensolver to large scale problems. We also plan to investigate a topology optimisation [33, 34, 35] for phononic/photonic crystals which have a wide bandgap by using the proposed methodology. It is also an interesting subject for solving eigenvalue problems related to non-linear PDEs, such as frequency dependent dependent absorbing photonic/phononic crystals.

[1] J Gazalet, S Dupont, JC Kastelik, Q Rolland, and B Djafari-Rouhani. A tutorial survey on waves propagating in periodic media: Electronic, photonic and phononic crystals. perception of the bloch theorem in both real and fourier domains. *Wave Motion*, Vol. 50, No. 3, pp. 619–654, 2013.

[2] KM Ho, CT Chan, and CM Soukoulis. Existence of a photonic gap in periodic dielectric structures. *Physical Review Letters*, Vol. 65, No. 25, p. 3152, 1990.

[3] MS. Kushwaha, P. Halevi, L. Dobrzynski, and B. Djafari-Rouhani. Acoustic band structure of periodic elastic composites. *Physical Review Letters*, Vol. 71, No. 13, p. 2022, 1993.
[4] M. Kafesaki and Eleftherios N. Economou. Multiple-scattering theory for three-dimensional periodic acoustic composites. *Physical review B*, Vol. 60, No. 17, p. 11993, 1999.
[5] Xindong Wang, X-G Zhang, Qingliang Yu, and BN Harmon. Multiple-scattering theory for electromagnetic waves. *Physical Review B*, Vol. 47, No. 8, p. 4161, 1993.
[6] K. Schmidt and P. Kauf. Computation of the band structure of two-dimensional photonic crystals with hp finite elements. *Computer Methods in Applied Mechanics and Engineering*, Vol. 198, No. 13, pp. 1249–1259, 2009.
[7] Feng-Lian Li, Yue-Sheng Wang, and Chuanzeng Zhang. Boundary element method for bandgap computation of photonic crystals. *Optics Communications*, Vol. 285, No. 5, pp. 527–532, 2012.
[8] Feng-Lian Li, Yue-Sheng Wang, Chuanzeng Zhang, and Gui-Lan Yu. Boundary element method for band gap calculations of two-dimensional solid phononic crystals. *Engineering Analysis with Boundary Elements*, Vol. 37, No. 2, pp. 225–235, 2013.
[9] Jianhua Yuan, Ya Yan Lu, and Xavier Antoine. Modeling photonic crystals by boundary integral equations and dirichlet-to-neumann maps. *Journal of Computational Physics*, Vol. 227, No. 9, pp. 4617–4629, 2008.
[10] Alex Barnett and Leslie Greengard. A new integral representation for quasi-periodic fields and its application to two-dimensional band structure calculations. *Journal of Computational Physics*, Vol. 229, No. 19, pp. 6898–6914, 2010.
[11] Tetsuya Sakurai and Hiroshi Sugiura. A projection method for generalized eigenvalue problems using numerical integration. *J. Comput. Appl. Math.*, Vol. 159, pp. 119–128, 2003.
[12] J. Asakura, T. Sakurai, H. Tadano, T. Ikegami, and K. Kimura. A numerical method for nonlinear eigenvalue problems using contour integrals. *JSIAM Letters*, Vol. 1, No. 0, pp. 52–55, 2009.
[13] Ben-Shan Liao, Zhaojun Bai, Lie-Quan Lee, and Kwok Ko. Nonlinear rayleigh-ritz iterative method for solving large scale nonlinear eigenvalue problems. *Taiwanese journal of mathematics*, Vol. 14, No. 3A, pp. pp–869, 2010.
[14] Elias Jarlebring, Wim Michiels, and Karl Meerbergen. The infinite arnoldi method and an application to time-delay systems with distributed delays. In *Time Delay Systems: Methods, Applications and New Trends*, pp. 229–239. Springer, 2012.
[15] Takashi Tsuchimochi, Masato Kobayashi, Ayako Nakata, Yutaka Imamura, and Hiromi Nakai. Application of the sakurai-sugiura projection method to core-excited-state calculation by time-dependent density functional theory. *Journal of computational chemistry*, Vol. 29, No. 14, pp. 2311–2316, 2008.
[16] Hiroshi Ohno, Yoshinobu Kuramashi, Tetsuya Sakurai, and Hiroto Tadano. A quadrature-based eigensolver with a krylov subspace method for shifted linear systems for hermitian eigenproblems in lattice qcd. *JSIAM Letters*, Vol. 2, No. 0, pp. 115–118, 2010.
[17] H. Gao, T. Matsumoto, T. Takahashi, and T. Yamada. Eigenvalue analysis for 2D acoustic problem by BEM with block SS method. *Transactions of JASCOME*, Vol. 11, p. 59, 2011.
[18] Haifeng Gao, Toshiro Matsumoto, Toru Takahashi, and Hiroshi Isakari. Eigenvalue analysis for acoustic problem in 3d by boundary element method with the block sakurai–sugiura method. *Engineering Analysis with Boundary Elements*, Vol. 37, No. 6, pp. 914–923, 2013.
[19] Ryota Misawa, Kazuki Niino, and Naoshi Nishimura. An FMM for waveguide problems of 2-D Helmholtz' equation and its application to eigenvalue problems. *Wave Motion*, Vol. 63, pp. 1–17, 2016.
[20] Wolf-Jürgen Beyn. An integral method for solving nonlinear eigenvalue problems. *Linear Algebra and Its Applications*, Vol. 436, No. 10, pp. 3839–3863, 2012.
[21] H-F. Gao, T. Matsumoto, T. Takahashi, and H. Isakari. Analysis of band structure for 2D acoustic phononic structure by BEM and the block SS method. *CMES: Computer Modeling in Engineering & Sciences*, Vol. 90, No. 4, pp. 283–301, 2013.
[22] V. Rokhlin. Rapid solution of intergral equations of classical potential theory. *Journal of Computational Physics*, Vol. 60, pp. 187–207, 1985.
[23] L. Greengard and V. Rokhlin. A fast algorithm for particle simulations. *Journal of Computational Physics*, Vol. 73, No. 2, pp. 325–348, 1987.
[24] PG. Martinsson and V. Rokhlin. A fast direct solver for boundary integral equations in two dimensions. *Journal*

of Computational Physics, Vol. 205, No. 1, pp. 1–23, 2005.
[25] M. Bebendorf. *Hierarchical matrices*. Springer, 2008.
[26] TP. Pals. *Multipole for scattering computations: Spectral discretization, stabilization, fast solvers*. PhD thesis, University of California Santa Barbara, 2004.
[27] H. Cheng, Z. Gimbutas, PG. Martinsson, and V. Rokhlin. On the compression of low rank matrices. *SIAM Journal on Scientific Computing*, Vol. 26, No. 4, pp. 1389–1404, 2005.
[28] AJ Burton and GF Miller. The application of integral equation methods to the numerical solution of some exterior boundary-value problems. *Proceedings of the Royal Society of London. A. Mathematical and Physical Sciences*, Vol. 323, No. 1553, pp. 201–210, 1971.
[29] Chang-Jun Zheng, Hai-Bo Chen, Hai-Feng Gao, and Lei Du. Is the burton–miller formulation really free of fictitious eigenfrequencies? *Engineering Analysis with Boundary Elements*, Vol. 59, pp. 43–51, 2015.
[30] S. Ohnuki and W.C. Chew. Numerical accuracy of multipole expansion for 2d mlfma. *Antennas and Propagation, IEEE Transactions on*, Vol. 51, No. 8, pp. 1883–1890, 2003.
[31] Kazuaki Sakoda. *Optical properties of photonic crystals*, Vol. 80. Springer Science & Business Media, 2004.
[32] AB Movchan and S Guenneau. Split-ring resonators and localized modes. *Physical Review B*, Vol. 70, No. 12, p. 125116, 2004.
[33] T. Yamada, K. Izui, S. Nishiwaki, and A. Takezawa. A topology optimization method based on the level set method incorporating a fictitious interface energy. *Computer Methods in Applied Mechanics and Engineering*, Vol. 199, No. 45, pp. 2876–2891, 2010.
[34] H. Isakari, K. Kuriyama, S. Harada, T. Yamada, T. Takahashi, and T. Matsumoto. A topology optimisation for three-dimensional acoustics with the level set method and the fast multipole boundary element method. *Mechanical Engineering Journal*, Vol. 1, No. 4, pp. CM0039–CM0039, 2014.
[35] G. Jing, H. Isakari, T. Matsumoto, T. Yamada, and T. Takahashi. Level set-based topology optimization for 2d heat conduction problems using bem with objective function defined on design-dependent boundary with heat transfer boundary condition. *Engineering Analysis with Boundary Elements*, Vol. 61, pp. 61–70, 2015.

Acknowledgements

This work was supported by JSPS Grant-in-Aid for Young Scientist (B) (Grant No. 26870269).